



THE UNIVERSITY *of* EDINBURGH

Edinburgh Research Explorer

Modeling of Complex Geometries and Boundary Conditions in Finite Difference/Finite Volume Time Domain Room Acoustics Simulation

Citation for published version:

Bilbao, S 2013, 'Modeling of Complex Geometries and Boundary Conditions in Finite Difference/Finite Volume Time Domain Room Acoustics Simulation', *IEEE Transactions on Audio, Speech and Language Processing*, vol. 21, no. 7, pp. 1524-1533. <https://doi.org/10.1109/TASL.2013.2256897>

Digital Object Identifier (DOI):

[10.1109/TASL.2013.2256897](https://doi.org/10.1109/TASL.2013.2256897)

Link:

[Link to publication record in Edinburgh Research Explorer](#)

Document Version:

Peer reviewed version

Published In:

IEEE Transactions on Audio, Speech and Language Processing

Publisher Rights Statement:

© Modeling of Complex Geometries and Boundary Conditions in Finite Difference/Finite Volume Time Domain Room Acoustics Simulation
Bilbao, S. Jul 2013 In : IEEE Transactions on Audio, Speech and Language Processing. 21, 7, p. 1524-1533 10 p.

General rights

Copyright for the publications made accessible via the Edinburgh Research Explorer is retained by the author(s) and / or other copyright owners and it is a condition of accessing these publications that users recognise and abide by the legal requirements associated with these rights.

Take down policy

The University of Edinburgh has made every reasonable effort to ensure that Edinburgh Research Explorer content complies with UK legislation. If you believe that the public display of this file breaches copyright please contact openaccess@ed.ac.uk providing details, and we will remove access to the work immediately and investigate your claim.



Modeling of Complex Geometries and Boundary Conditions in Finite Difference/Finite Volume Time Domain Room Acoustics Simulation

Stefan Bilbao

Abstract—Due to recent increases in computing power, room acoustics simulation in 3D using time stepping schemes is becoming a viable alternative to standard methods based on ray tracing and the image source method. Finite Difference Time Domain (FDTD) methods, operating over regular grids, are perhaps the best known among such methods, which simulate the acoustic field in its entirety over the problem domain. In a realistic room acoustics setting, working over a regular grid is attractive from a computational standpoint, but is complicated by geometrical considerations, particularly when the geometry does not conform neatly to the grid, and those of boundary conditions which emulate the properties of real wall materials. Both such features may be dealt with through an appeal to methods operating over unstructured grids, such as finite volume methods, which reduce to FDTD when employed over regular grids. Through numerical energy analysis, such methods lead to direct stability conditions for complex problems, including convenient geometrical conditions at irregular boundaries. Simulation results are presented.

Index Terms—Finite difference time domain method, finite volume methods, room acoustics.

I. INTRODUCTION

ROOM acoustics simulation, for purposes of auditioning of virtual spaces, or artificial reverberation is a subject of continuing interest. Many techniques currently in use rely on ray-based formulations [1] or image source techniques [2], [3]; other techniques used for analysis purposes include methods such as the functional transformation method [4], and frequency domain methods such as the finite element method [5], [6], and boundary element methods [7]–[9].

Full simulation of acoustic spaces in the time domain is now coming within reach in specialized hardware (such as, e.g., GPGPUs [10]–[14]), allowing for much more accurate rendering. In such approaches, the acoustic field is simulated in its entirety over the entire problem domain (i.e., the room), and a technique frequently used is the finite difference time domain method (FDTD) [15]–[17], or equivalent digital waveguide mesh algorithms [18]–[20]—as they operate over a regular grid, these techniques have many benefits from the point of view of

parallelization. Such techniques are inherently local, leading to simple algorithm structure and updates in contrast with other non-local time domain methods (such as pseudo spectral methods, which have great benefits in terms of accuracy, and which have been applied in room acoustics simulation [21].

In practice, such local schemes are to be used over realistic room geometries, for which the problem domain does not align well with a regular grid, and where nontrivial impedance boundary conditions are employed. One of the major difficulties been in determining stability conditions in these cases. An appeal to methods defined over unstructured grids can be very useful in this regard, even if over the problem interior, the algorithm is to be implemented over a structured grid. A well-known example of such an unstructured method is the finite volume technique, based on discrete conservation laws, which is amenable to stability analysis even under highly irregular and realistic boundary conditions, and is a flexible alternative to fitted boundary techniques used exclusively with regular FDTD schemes [22], [23]. Botteldooren [31] used the framework of conservation laws in an early investigation of FDTD methods over quasi-Cartesian grids.

Standard FDTD stability checking techniques such as von Neumann analysis [24], which are based on spatial Fourier domain and temporal frequency domain concepts are often used to arrive at necessary stability conditions for FDTD methods, operating over regular grids. When an irregular boundary is imposed, and when boundary conditions are nontrivial, as in the case of realistic impedances, it becomes difficult to arrive at rigorous conditions for stability (certain extensions, such as GKS theory [25], can be used to find stability conditions for simple geometries such as half- or quarter-spaces). In the interest of allowing practical, stable designs under realistic conditions, a technique that will be employed here, for stability analysis, is the maintenance of strict energy conservation, leading to a direct bound on solution growth in the time domain. Such techniques are used directly in the time domain, and may be used over unstructured grids—in particular, there is no use of frequency domain concepts. When specialized to Cartesian grids, such methods yield the same stability conditions as von Neumann methods—but also include the effects of boundary conditions.

The first order system describing the evolution of the acoustic field is given in Section II, along with the reduced second order system, as well as passive boundary conditions suitable in the context of room modeling. The finite volume technique for the acoustic wave equation is introduced in Section III. Various implementation details, especially in the case of complex geome-

Manuscript received January 10, 2013; revised March 26, 2013; accepted March 27, 2013. Date of publication April 04, 2013; date of current version nulldate. This work was supported by the European Research Council, under Grant StG-2011-279068-NESS. The associate editor coordinating the review of this manuscript and approving it for publication was Prof Lauri Savioja.

The author is with the Acoustics and Audio Group, University of Edinburgh, Edinburgh EH9 3JZ, U.K. (e-mail: sbilbao@staffmail.ed.ac.uk).

Digital Object Identifier 10.1109/TASL.2013.2256897

tries appear in Section IV, and simulation results are presented in Section V.

II. THE WAVE EQUATION AND IMPEDANCE BOUNDARY CONDITIONS

A. Acoustic Wave Propagation

The acoustic field within a d dimensional enclosure can be described in terms of pressure $p = p(\mathbf{x}, t)$ and particle velocity $\mathbf{v}(\mathbf{x}, t)$ as

$$\frac{1}{\rho c^2} \frac{\partial p}{\partial t} = -\nabla \cdot \mathbf{v} \quad (1a)$$

$$\rho \frac{\partial \mathbf{v}}{\partial t} = -\nabla p \quad (1b)$$

Here, t is time, and \mathbf{x} represents position in a d dimensional space, and is confined to a region $\mathbf{x} \in \mathcal{V} \subset \mathbb{R}^d$. ρ is density, c is wave speed and ∇ and $\nabla \cdot$ are the d dimensional gradient and divergence operations, respectively. Though it is the $d = 3$ case which is ultimately of interest in room acoustics applications, the construction of finite volume methods is insensitive to the choice of d and thus 2D problems will be examined here subsequently as test cases.

A single scalar boundary condition must be supplied over the boundary $\partial\mathcal{V}$ of the region. To this end, note that by multiplying (1a) by p and integrating over \mathcal{V} , and making use of the divergence theorem, the following energy balance results:

$$\frac{d}{dt} \left(\int_{\mathcal{V}} \frac{1}{2\rho c^2} p^2 + \frac{\rho}{2} |\mathbf{v}|^2 d\mathbf{x} \right) = - \int_{\partial\mathcal{V}} p v_n d\sigma \quad (2)$$

where $v_n = \mathbf{n} \cdot \mathbf{v}$ is the component of velocity outward normal to the $(d-1)$ dimensional boundary $\partial\mathcal{V}$ of the volume \mathcal{V} (with outward normal vector \mathbf{n}) and $d\sigma$ is a $(d-1)$ -dimensional differential element, or as

$$\frac{d}{dt} \mathcal{H}_{(i)} = -\mathcal{B} \quad (3)$$

where $\mathcal{H}_{(i)} = \mathcal{H}_{(i)}(t) \geq 0$ is the total energy contained in the acoustic field, and where $\mathcal{B} = \mathcal{B}(t)$ is a term representing power outflow.

B. Second Order Wave Equation

The system (1) is often written in a second order form. The natural representation [26] is in terms of a velocity potential Ψ :

$$\frac{\partial^2 \Psi}{\partial t^2} = c^2 \nabla^2 \Psi \quad (4)$$

where

$$p = \rho \frac{\partial \Psi}{\partial t} \quad \mathbf{v} = -\nabla \Psi \quad (5)$$

and where ∇^2 is the d dimensional Laplacian operator. In this second order form, the energy balance (2) may be written in terms of Ψ as

$$\frac{d}{dt} \left(\int_{\mathcal{V}} \frac{\rho}{2c^2} \left(\frac{\partial \Psi}{\partial t} \right)^2 + \frac{\rho}{2} |\nabla \Psi|^2 d\mathbf{x} \right) = \int_{\partial\mathcal{V}} \rho \frac{\partial \Psi}{\partial t} \mathbf{n} \cdot \nabla \Psi d\sigma \quad (6)$$

C. Impedance Boundary Conditions

In room acoustics applications, it is usually passive terminations, or wall conditions which are of interest. In this case, one requires that

$$\mathcal{B} = \mathcal{Q} + \frac{d}{dt} \mathcal{H}_{(b)} \quad (7)$$

where $\mathcal{Q} = \mathcal{Q}(t) \geq 0$ represents dissipation, and where $\mathcal{H}_{(b)} = \mathcal{H}_{(b)}(t) \geq 0$ is energy stored at the room boundary. It then follows that the energy balance may be written as

$$\frac{d}{dt} \mathcal{H} = -\mathcal{Q} \leq 0 \quad (8)$$

where the total energy $\mathcal{H} = \mathcal{H}_{(i)} + \mathcal{H}_{(b)} \geq 0$ is non-increasing over time.

Examining the power term \mathcal{B} from (3), this will be true if pressure p and the outward normal component of the velocity are related, in the frequency domain, by a positive real impedance [27], corresponding to a passive boundary condition. One particularly simple case is that of a parallel stiffness/inertance/resistive termination, given by

$$v_n = Y_0 \left(A \frac{d}{dt} p + Bp + Cm \right) \quad \frac{d}{dt} m = p \quad (9)$$

over $\partial\mathcal{V}$ where $Y_0 = 1/\rho c$ is the characteristic admittance of air, and where A , B and C are non-negative functions defined over the boundary. In this case, the loss \mathcal{Q} and stored boundary energy \mathcal{B} are given by

$$\mathcal{Q} = Y_0 \int_{\partial\mathcal{V}} B p^2 d\sigma \geq 0 \quad \mathcal{H}_{(b)} = \frac{Y_0}{2} \int_{\partial\mathcal{V}} A p^2 + C m^2 d\sigma \geq 0 \quad (10)$$

The complementary case is that of a series stiffness/inertance/resistive termination, given by

$$p = Z_0 \left(D \frac{d}{dt} v_n + E v_n + Fg \right) \quad \frac{d}{dt} g = v_n \quad (11)$$

over $\partial\mathcal{V}$ where $Z_0 = \rho c$ is the characteristic impedance of air, and where D , E and F are non-negative functions defined over the boundary. In this case, the loss \mathcal{Q} and stored boundary energy \mathcal{B} are given by

$$\mathcal{Q} = Z_0 \int_{\partial\mathcal{V}} E v_n^2 d\sigma \geq 0 \quad \mathcal{H}_{(b)} = \frac{Z_0}{2} \int_{\partial\mathcal{V}} D v_n^2 + F g^2 d\sigma \geq 0 \quad (12)$$

In both cases, the system is passive as long as A , B , C (or D , E and F) are constant in time and non-negative, though they may be variable over the room boundary $\partial\mathcal{V}$, allowing for variation in wall properties with location.

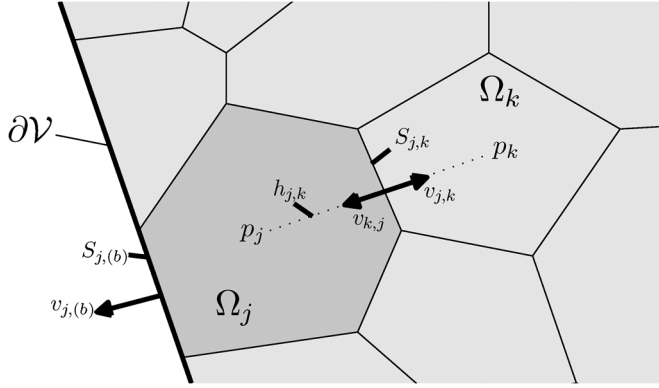


Fig. 1. Tiling of a 2D region \mathcal{V} , with boundary $\partial\mathcal{V}$ as indicated. Two cells, Ω_j and Ω_k are shown, with associated pressures p_j and p_k , as well as the pair of normal velocities $v_{j,k} = -v_{k,j}$ at the common edge, of area $S_{j,k}$. An average distance between cell centroids is shown as $h_{j,k}$. Cell Ω_j possesses a boundary, of area $S_{j,(b)}$, with associated outward normal velocity $v_{j,(b)}$.

These are locally reactive conditions, meaning that they may be characterized in terms of an impedance which is independent of the angle of incidence (which is not generally the case) [28]. Non-locally reactive conditions necessarily involve spatial derivatives tangential to the boundary, but must also satisfy the conditions $\mathcal{H}_{(b)} \geq 0$ and $\mathcal{Q} \geq 0$.

III. FINITE VOLUME METHODS

Finite volume methods have a long history of use in problems in electromagnetics [29] and aeroacoustics, and are based on discretizations of conservation laws; for an introduction to finite volume methods, see the text by Leveque [30]. Botteldooren [31], though not employing finite volume methods directly, has developed FDTD methods over quasi-Cartesian grids using conservation laws.

A. Cells

Consider a tiling of the d dimensional volume \mathcal{V} by N polyhedral cells Ω_j , $j = 1, \dots, N$. For two adjacent cells Ω_j and Ω_k , the $(d-1)$ dimensional surface area of the adjoining face is written as $S_{j,k} = S_{k,j}$, and the mean distance between the adjacent cells is $h_{j,k} = h_{k,j}$. V_j denotes the d dimensional volume of cell Ω_j . See Fig. 1, showing a typical tiling in 2D.

B. Spatial Discretization

To arrive at a finite volume discretization, the first step is to approximate the system (1) over cells. To this end, integrate (1a) over the cell Ω_j , to get, again using the divergence theorem,

$$\frac{1}{\rho c^2} \frac{d}{dt} \int_{\Omega_j} p d\mathbf{x} = - \int_{\partial\Omega_j} v_n d\sigma \quad (13)$$

where v_n represents the component of the velocity \mathbf{v} outward normal to the boundary $\partial\Omega_j$. In order to arrive at a discretization operating over a finite set of values for the pressure and

velocity fields, the following approximate discrete set of values is defined. An average pressure p_j over cell Ω_j is defined as

$$p_j = \frac{1}{V_j} \int_{\Omega_j} p d\mathbf{x} \quad (14)$$

If $v_{j,k}$ represents an outward normal velocity directed towards an adjacent cell Ω_k , averaged over the common face, of area $S_{j,k}$, then

$$\int_{\partial\Omega_j} v_n d\sigma = \sum_{k=1}^N S_{j,k} q_{j,k} v_{j,k} \quad (15)$$

where $q_{j,k}$ is an indicator function taking the value 1 for Ω_j and Ω_k adjacent, and 0 otherwise. Note that $v_{j,k} = -v_{k,j}$ (reflecting conservation, and leading to a skew symmetry property [32] in the resulting energy analysis).

A semi-discrete approximation to (1a) is then

$$\frac{V_j}{\rho c^2} \frac{d}{dt} p_j = - \sum_{k=1}^N S_{j,k} q_{j,k} v_{j,k} - S_{j,(b)} q_{j,(b)} v_{j,(b)} \quad (16)$$

where here, boundary terms have been included: At a cell Ω_j with a face adjacent to the boundary of the room (of area $S_{j,(b)}$), $v_{j,(b)}$ represents outward normal velocity, and $q_{j,(b)}$ is an indicator function taking on the value 1 for a cell Ω_j with such a boundary face, and the value 0 otherwise. (It is assumed here, for simplicity, that a boundary cell possesses a single boundary face—in the case of, example, approximation with square or cubic elements, such as a staircase approximation, the two or more unadjoined faces may be coalesced into a single boundary face with an area which is the sum of those of the unadjoined faces.)

Similarly, (1b) may then be approximated as

$$\rho \frac{d}{dt} v_{j,k} = - \frac{1}{h_{j,k}} (p_k - p_j) \quad (17)$$

where only the values $v_{j,k}$ between adjacent cells Ω_j and Ω_k need be considered (and stored in implementation).

C. Interleaved Time Discretization

In a discrete time implementation it is convenient to use interleaved approximations to p_j and $v_{j,k}$. For a given sample rate F_s , and time step $T_s = 1/F_s$, define the approximations p_j^n and $v_{j,k}^{n+1/2}$ as

$$p_j^n \approx p_j(nT_s) \quad v_{j,k}^{n+1/2} \approx v_{j,k}((n+1/2)T_s) \quad (18)$$

The use of the same notation for the fully discrete and semi-discrete cases should not cause confusion, as only the fully discrete case will be considered in the remainder of this article.

D. Difference and Averaging Operators, and Identities

Shift operations e_+ and e_- are defined as

$$\begin{aligned} e_+ p_j^n &= p_j^{n+1} & e_- p_j^n &= p_j^{n-1} \\ e_+ v_{j,k}^{n-1/2} &= v_{j,k}^{n+1/2} & e_- v_{j,k}^{n+1/2} &= v_{j,k}^{n-1/2} \end{aligned} \quad (19)$$

$$\begin{aligned} e_+ p_j^n &= p_j^{n+1} & e_- p_j^n &= p_j^{n-1} \\ e_+ v_{j,k}^{n-1/2} &= v_{j,k}^{n+1/2} & e_- v_{j,k}^{n+1/2} &= v_{j,k}^{n-1/2} \end{aligned} \quad (20)$$

Approximations δ_+ and δ_- to the time derivative d/dt may be defined as

$$\delta_+ = \frac{1}{T_s}(e_+ - 1) \quad \delta_- = \frac{1}{T_s}(1 - e_-) \quad (21)$$

and averaging operations μ_+ and μ_- as

$$\mu_+ = \frac{1}{2}(e_+ + 1) \quad \mu_- = \frac{1}{2}(1 + e_-) \quad (22)$$

For any time series f , the following identities hold:

$$(\mu_+ f)(\delta_+ f) = \delta_+ \left(\frac{1}{2} f^2 \right) \quad f \mu_+ \delta_- f = \delta_+ \left(\frac{1}{2} f e_- f \right) \quad (23)$$

Furthermore, the following inequality holds:

$$f e_- f \geq -\frac{T_s^2}{4} (\delta_- f)^2 \quad (24)$$

E. A Fully Discrete Scheme

A fully discrete approximation to system (1) may then be written, by replacing time derivatives in (16) and (17) by difference operations, as

$$\frac{V_j}{\rho c^2} \delta_+ p_j = - \sum_{k=1}^N S_{j,k} q_{j,k} v_{j,k} - S_{j,(b)} q_{j,(b)} v_{j,(b)} \quad (25)$$

$$\rho \delta_- v_{j,k} = - \frac{1}{h_{j,k}} (p_k - p_j) \quad (26)$$

In this condensed operator formulation, instances of p_j and $v_{j,k}$ are assumed to refer to values p_j^n and $v_{j,k}^{n+1/2}$ at time step n , and $n+1/2$, respectively. This scheme is fully explicit over the problem interior; the boundary velocity approximations $v_{j,(b)}$ will be specified shortly.

Defining a set of discrete velocity potentials Ψ_j by

$$p_j = \rho \delta_- \Psi_j \quad (27)$$

one can arrive at a second order scheme analogous to (4):

$$\frac{V_j}{\rho c^2} \delta_+ \delta_- \Psi_j = \sum_{k=1}^N \frac{S_{j,k} q_{j,k}}{\rho h_{j,k}} (\Psi_k - \Psi_j) - S_{j,(b)} q_{j,(b)} v_{j,(b)} \quad (28)$$

F. An Energy Balance

Energy techniques are a useful means of arriving at bounds on solution growth; such techniques are used in the semi-discrete case for unstructured finite volume methods in [32], and are extended here to the case of a fully discrete method.

In analogy with the energy analysis in Section II, one may multiply (25) by $\mu_+ p_j$, and sum over the ensemble of cells $j = 1, \dots, N$ to give

$$\sum_{j=1}^N \frac{V_j}{\rho c^2} \mu_+ p_j \delta_+ p_j = - \underbrace{\sum_{j=1}^N \sum_{k=1}^N S_{j,k} q_{j,k} \mu_+ p_j v_{j,k}}_W - \mathbf{b} \quad (29)$$

where the boundary term \mathbf{b} is given by

$$\mathbf{b} = \sum_{j=1}^N S_{j,(b)} q_{j,(b)} \mu_+ p_j v_{j,(b)} \quad (30)$$

One may write, by symmetry, for the term W above,

$$W = \frac{1}{2} \sum_{j=1}^N \sum_{k=1}^N S_{j,k} q_{j,k} \mu_+ p_j v_{j,k} + S_{k,j} q_{k,j} \mu_+ p_k v_{k,j} \quad (31)$$

and furthermore, using $S_{j,k} = S_{k,j}$, $q_{j,k} = q_{k,j}$, $v_{j,k} = -v_{k,j}$, and the second member (26) of the discrete scheme,

$$W = \frac{1}{2} \sum_{j=1}^N \sum_{k=1}^N S_{j,k} q_{j,k} \mu_+ (p_j - p_k) v_{j,k} \quad (32)$$

$$= \frac{\rho}{2} \sum_{j=1}^N \sum_{k=1}^N S_{j,k} h_{j,k} q_{j,k} v_{j,k} \mu_+ \delta_- v_{j,k} \quad (33)$$

Finally, using the identities (23), one arrives at the discrete time energy balance

$$\delta_+ \mathfrak{h}_{(i)} = -\mathbf{b} \quad (34)$$

where the time series $\mathfrak{h}_{(i)} = \mathfrak{h}_{(i)}^n$ is given by

$$\mathfrak{h}_{(i)} = \sum_{j=1}^N \left(\frac{V_j}{2\rho c^2} (p_j)^2 + \frac{\rho}{4} \sum_{k=1}^N S_{j,k} h_{j,k} q_{j,k} v_{j,k} e_- v_{j,k} \right) \quad (35)$$

and again represents the stored energy in the problem interior.

G. Discrete Impedance Boundary Conditions

In order that the full scheme remain numerically passive, it is necessary that the numerical boundary conditions satisfy a dissipative property analogous to that of the continuous case. In the case of the specialized impedance condition given in (9), consider the following discretization:

$$v_{j,(b)} = Y_0 (A_j \delta_+ p_j + B_j \mu_+ p_j + C_j \mu_+ m_j) \quad (36a)$$

$$\delta_+ m_j = \mu_+ p_j \quad (36b)$$

for some constants $A_j, B_j, C_j \geq 0$, and where a new set of boundary values $m_j = m_j^n$ has been introduced in order to store energy.

Using the first of identities (23), the boundary term \mathbf{b} can then be written as

$$\mathbf{b} = \mathbf{q} + \delta_+ \mathfrak{h}_{(b)} \quad (37)$$

where

$$\mathfrak{q} = Y_0 \sum_{j=1}^N B_j S_{j,(b)} q_{j,(b)} (\mu_+ p_j)^2 \geq 0 \quad (38)$$

$$\mathfrak{h}_{(b)} = \frac{Y_0}{2} \sum_{j=1}^N S_{j,(b)} q_{j,(b)} (A_j (p_j)^2 + C_j (m_j)^2) \geq 0 \quad (39)$$

Under the complementary boundary condition (11), one may use, instead, $v_{j,(b)} = \mu_+ \hat{v}_{j,(b)}$, where

$$\mu_+ p_j = Z_0 (D_j \delta_+ \hat{v}_{j,(b)} + E_j \mu_+ \hat{v}_{j,(b)} + F_j \mu_+ g_j) \quad (40a)$$

$$\delta_+ g_j = \mu_+ \hat{v}_{j,(b)} \quad (40b)$$

for some constants $D_j, E_j, F_j \geq 0$, and where a new set of boundary values $g_j = g_j^n$ has been introduced in order to store energy.

Now, one again has an energy relationship of the form (37), but with

$$\mathfrak{q} = Z_0 \sum_{j=1}^N E_j S_{j,(b)} q_{j,(b)} (\mu_+ \hat{v}_{j,(b)})^2 \geq 0 \quad (41)$$

$$\begin{aligned} \mathfrak{h}_{(b)} &= \frac{Z_0}{2} \sum_{j=1}^N S_{j,(b)} q_{j,(b)} (D_j (\mu_+ \hat{v}_{j,(b)})^2 + F_j (g_j)^2) \\ &\geq 0 \end{aligned} \quad (42)$$

H. Stability Conditions

Under either the parallel or series conditions described above, in the end, one has for the initial value problem,

$$\delta_+ \mathfrak{h} = -\mathfrak{q} \leq 0 \quad \implies \quad \mathfrak{h}^n \leq \mathfrak{h}^{n-1} \leq \mathfrak{h}^0 \quad (43)$$

where $\mathfrak{h} = \mathfrak{h}_{(i)} + \mathfrak{h}_{(b)}$ is the total numerical energy of the scheme. Thus total energy is monotonically decreasing with time.

All that remains, from the point of view of stability analysis, is to show conditions under which the internal stored energy $\mathfrak{h}_{(i)}$ is non-negative. To this end, using the inequality (24),

$$\mathfrak{h}_{(i)} \geq \sum_{j=1}^N \left(\frac{V_j}{2\rho c^2} (p_j)^2 - \frac{\rho T_s^2}{16} \sum_{k=1}^N S_{j,k} h_{j,k} q_{j,k} (\delta_- v_{j,k})^2 \right) \quad (44)$$

and from (26),

$$\mathfrak{h}_{(i)} \geq \sum_{j=1}^N \left(\frac{V_j}{2\rho c^2} (p_j)^2 - \frac{T_s^2}{16\rho} \sum_{k=1}^N \frac{S_{j,k}}{h_{j,k}} q_{j,k} (p_k - p_j)^2 \right) \quad (45)$$

$$\geq \sum_{j=1}^N \left(\frac{V_j}{2\rho c^2} (p_j)^2 - \frac{T_s^2}{8\rho} \sum_{k=1}^N \frac{S_{j,k}}{h_{j,k}} q_{j,k} (p_k^2 + p_j^2) \right) \quad (46)$$

and finally, by symmetry over the double summation,

$$\mathfrak{h}_{(i)} \geq \sum_{j=1}^N \left(\frac{V_j}{2\rho c^2} - \frac{T_s^2}{4\rho} \sum_{k=1}^N \frac{S_{j,k}}{h_{j,k}} q_{j,k} \right) p_j^2 \quad (47)$$

The internal stored energy in the acoustic field is thus non-negative under the conditions

$$\frac{V_j}{2c^2} - \frac{T_s^2}{4} \sum_{k=1}^N \frac{S_{j,k}}{h_{j,k}} q_{j,k} \geq 0 \quad j = 1, \dots, N \quad (48)$$

Under this condition, one has, then, for an initial value problem,

$$0 \leq \mathfrak{h}_{(i)}^n \leq \mathfrak{h}^n \leq \mathfrak{h}^0 \quad (49)$$

and thus the internal stored energy (itself a positive semi-definite function of the state) may be bounded in terms of the initial energy, assumed to be finite.

The condition (48) may thus be viewed as a sufficient stability condition for the entire scheme. Furthermore, it is based solely on geometric considerations which may be easily verified at every cell in the domain. Though it is a necessary condition as well for several typical FDTD schemes (and reduces to conditions arrived at through standard methods such as, e.g., von Neumann analysis), in some cases it is not—this point will be discussed, with reference to schemes operating over hexagonal grids, in the next section.

IV. IMPLEMENTATION DETAILS AND REDUCTION TO FDTD SCHEMES

A. Explicit Update Form

At an internal cell Ω_j (i.e., one not possessing a boundary), the updates (25) and (26) may be written, in terms of time series p_j^n and $v_{j,k}^{n+1/2}$, as

$$p_j^{n+1} = p_j^n - \frac{\rho c^2 T_s}{V_j} \sum_{k=1}^N S_{j,k} q_{j,k} v_{j,k}^{n+1/2} \quad (50)$$

$$v_{j,k}^{n+1/2} = v_{j,k}^{n-1/2} - \frac{T_s}{\rho h_{j,k}} (p_k^n - p_j^n) \quad (51)$$

and similarly, a second order update in the velocity potential Ψ_j^n may be written as

$$\Psi_j^{n+1} = 2\Psi_j^n - \Psi_j^{n-1} + \frac{T_s^2 c^2}{V_j} \sum_{k=1}^N \frac{S_{j,k} q_{j,k}}{h_{j,k}} (\Psi_k^n - \Psi_j^n) \quad (52)$$

B. Explicit Boundary Updates

Consider the parallel boundary condition (9). At a cell Ω_j with a boundary, in the first order form, the updates (25) and

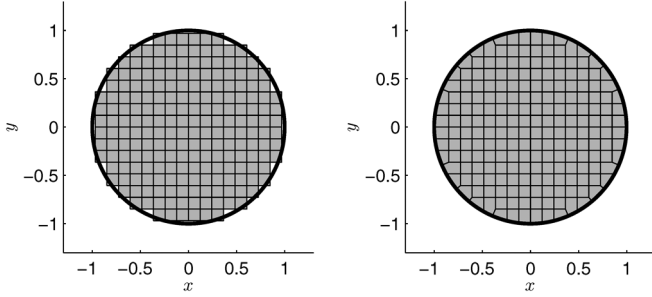


Fig. 2. Two distinct tilings of a circular region, where the interior cells are squares on a rectangular grid: Left: Staircase approximation; Right: Fitted boundary cells.

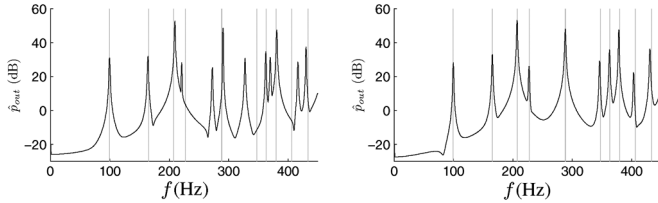


Fig. 3. Fourier transform \hat{p}_{out} (in dB) of pressure output response from a simulation over a circular domain, using a staircase boundary approximation (left) and fitted boundary cells (right). Exact modal frequencies for the circular enclosure are indicated by gray lines.

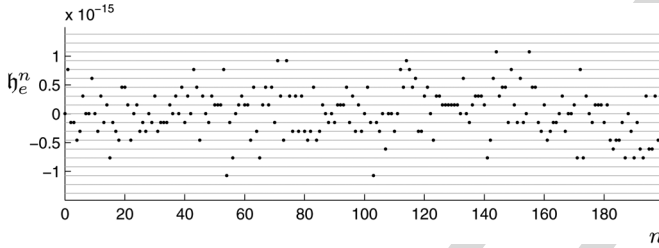


Fig. 4. Variation in numerical energy $h_e^n = (h^n - h^0)/h^0$ for the Cartesian scheme operating over a circular region, with fitted boundary cells as illustrated at right in Fig. 2. In this case the initial conditions are set to those corresponding to an impulse in the problem interior. Gray lines indicate multiples of machine error in double precision floating point arithmetic, showing numerical losslessness of the simulation.

(36) may be combined to give a pair of updates in the time series p_j^n and m_j^n :

$$p_j^{n+1} = \frac{\alpha_j}{\gamma_j} p_j^n - \frac{1}{\gamma_j} \sum_{k=1}^N S_{j,k} q_{j,k} v_{j,k}^{n+1/2} - \frac{\beta_j}{\gamma_j} m_j^n \quad (53)$$

$$m_j^{n+1} = m_j^n + \frac{k}{2} (p_j^{n+1} + p_j^n) \quad (54)$$

where

$$\alpha_j = \frac{V_j}{\rho c^2 T_s} + S_{j,(b)} Y_0 \left(\frac{A_j}{T_s} - \frac{B_j}{2} - \frac{C_j T_s}{4} \right) \quad (55)$$

$$\beta_j = S_{j,(b)} Y_0 C_j \quad (56)$$

$$\gamma_j = \frac{V_j}{\rho c^2 T_s} + S_{j,(b)} Y_0 \left(\frac{A_j}{T_s} + \frac{B_j}{2} + \frac{C_j T_s}{4} \right) \quad (57)$$

This pair of updates is explicit if performed in the order shown (leading to a small degree of serial computation at the boundary). It is interesting to note that the second order form is particularly convenient with this boundary condition, as no additional state is required at the boundary.

The case of the series condition (11) is similar, leading also to an explicit pair of updates at the boundary cells, but is omitted here due to space considerations; in this case (as with virtually any other reasonably complex boundary condition), additional state will be required at the boundary.

C. Standard Schemes in 2D and 3D

If, in 2D, the cells Ω_j are chosen as squares of side length $S_{j,k} = h$, then $V_j = h^2$, and $h_{j,k} = h$. The simplest possible second order explicit scheme for the 2D wave equation results, employing nearest neighbors. The scheme, written in terms of velocity potential $\Psi_{l,m}^n$ (indexed now by l and m) is, at an interior cell,

$$\delta_+ \delta_- \Psi_{l,m} = c^2 (\Psi_{l+1,m} + \Psi_{l-1,m} + \Psi_{l,m+1} + \Psi_{l,m-1} - 4\Psi_{l,m}) \quad (58)$$

The condition (48), evaluated at an interior cell, gives the standard stability condition

$$cT_s/h \leq 1/\sqrt{2} \quad (59)$$

which is usually arrived at using frequency domain techniques (von Neumann analysis [24]).

An interesting case is that of regular hexagonal cells, giving rise to a second order scheme for which each velocity potential value is updated using six nearest neighbors (assumed a distance h away) [33]. In this case, the sufficient stability condition, from (48), is $cT_s/h \leq 1/\sqrt{2}$; but, from von Neumann analysis, the necessary condition is $cT_s/h \leq \sqrt{2/3}$, which is less strict. More comments on this appear in Section VI.

Similarly, in 3D, the cells Ω_j can be chosen as cubes of side length $h_{j,k} = h$, and thus $S_{j,k} = h^2$ and $V_j = h^3$. The standard seven point second order explicit scheme for the 3D wave equation results, employing nearest neighbors. The second order form, written in terms of velocity potential $\Psi_{l,m}^n$ (indexed now by l , m and p) is

$$\delta_+ \delta_- \Psi_{l,m,p} = c^2 (\Psi_{l+1,m,p} + \Psi_{l-1,m,p} + \Psi_{l,m+1,p} + \Psi_{l,m-1,p} + \Psi_{l,m,p+1} + \Psi_{l,m,p-1} - 6\Psi_{l,m}) \quad (60)$$

The condition (48), evaluated at an interior cell, again gives the standard stability condition

$$cT_s/h \leq 1/\sqrt{3} \quad (61)$$

V. SIMULATION RESULTS

In this section, various simulation results are presented, in both 2D and 3D, illustrating the properties of such schemes, as described previously, including comparisons of different tilings, energy conservation, and variable reflectance properties at boundaries.

A. Circular Region in 2D

As a very simple test case of a geometry which does not conform neatly to a Cartesian grid, consider a circular enclosure in a 2D plane, where a simple rectangular FDTD scheme is

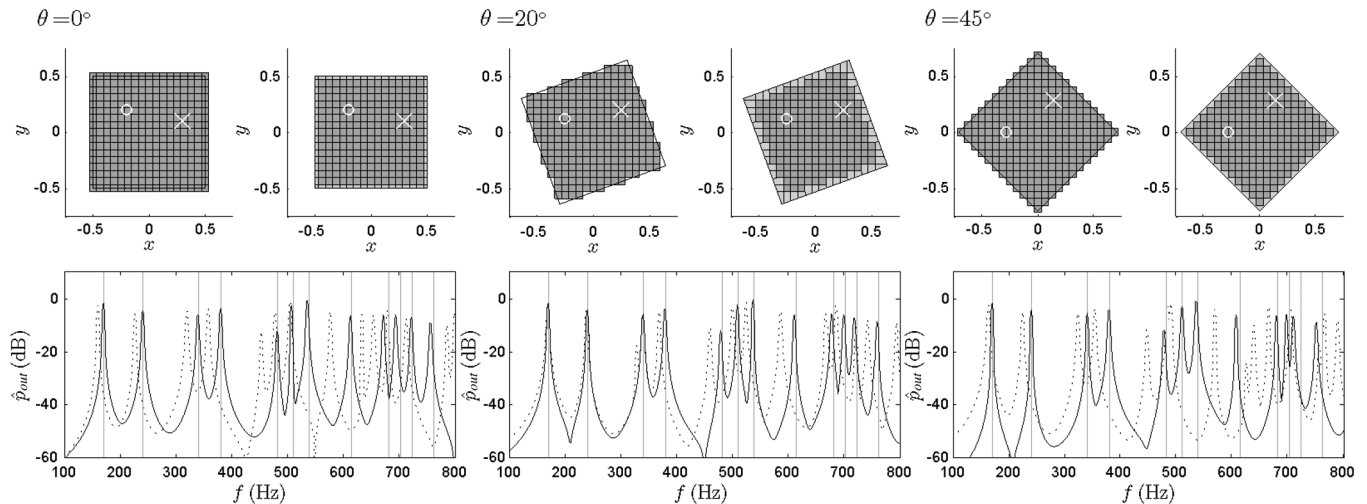


Fig. 5. Rotated square, of side length 1 m, discretized over a regular Cartesian grid not aligned with the rotation, using a staircase approximation, and fitted boundary cells (top row). Frequency responses, for excitation/readout points indicated by \circ and \times respectively, are shown in the bottom row, for the staircase approximation (dotted) and fitted cells (solid). Exact modal frequencies, under perfectly reflective boundary conditions, are shown as gray lines. The sample rate is 8 kHz.

employed over the grid interior. Two distinct tilings, namely a simple “staircase” approximation, and a fitted grid, using quadrilateral and pentagonal cells at the boundaries, are shown in Fig. 2. In this case the circular region is of radius 1 m, the sample rate is chosen as 4 kHz, and the wave speed is $c = 340$ m/s.

Under purely reflective conditions at the boundary (i.e., $v_{j,(b)} = 0$ for all boundary cells), it is useful to examine the response of the enclosure to an impulsive excitation, exciting the various modal frequencies (which, for this geometry and these boundary conditions, may be calculated explicitly). Fig. 3 shows the Fourier transforms of these responses, in the case of a staircase tiling, and a fitted boundary tiling, as illustrated in Fig. 2. The fitted tiling gives a much better match to the theoretical modal frequencies, with deviations appearing in both cases at higher frequencies, reflecting numerical dispersion of the scheme itself [34].

In either case the scheme is energy conserving (lossless and passive), including boundary termination, to machine accuracy. See Fig. 4, illustrating variation in the least significant bit of the total energy, in double precision floating point arithmetic.

B. Rotated Rectangular Region in 2D

As another example, consider the case of a square region, of side length 1 m, under various angles of rotation, as shown at top in Fig. 5. Again, it is useful to examine plots of frequency responses under perfectly reflective boundary conditions, in the cases of a staircase approximation to the square over the grid, and an approximation using fitted cells. As can be seen from the frequency responses, even at a relatively high sample rate (in this case 8 kHz), the low modal frequencies for the staircase approximation deviate significantly from theoretical values, whereas for the approximation using fitted cells, the response remains relatively independent of the rotation angle of the square.

By symmetry, the wave equation defined over a square geometry possesses doubled, or degenerate modes at a series of

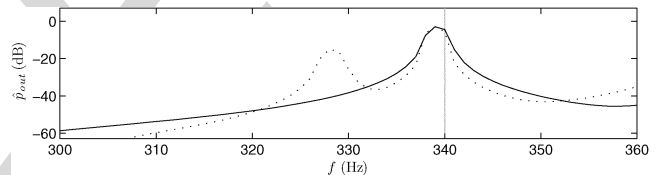


Fig. 6. Detail of Fig. 5, for a rotation angle of 20° , illustrating a numerically split degenerate mode pair in the case of the staircase approximation (dotted line) compared with the response for fitted boundary cells (solid line). The exact frequency of the mode pair is 340 Hz, indicated by a gray line. The fitted boundary approximation gives a pair of frequencies at 339 Hz, and for the staircase approximation, these are split to 339 Hz and 328.7 Hz.

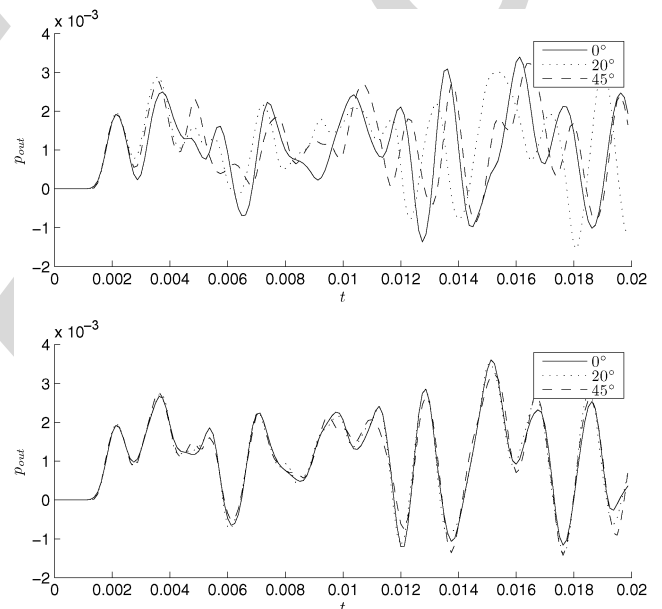


Fig. 7. Time response for the system described in Fig. 5, under an excitation of a raised cosine, of duration 2 ms for the staircase approximation (top) and for fitted boundary cells (bottom). Responses are shown for angles of rotation of 0° (solid line), 20° (dotted line) and 45° (dashed line).

frequencies. Numerically, however, this symmetry can be disturbed, depending on the type of discretization employed at the

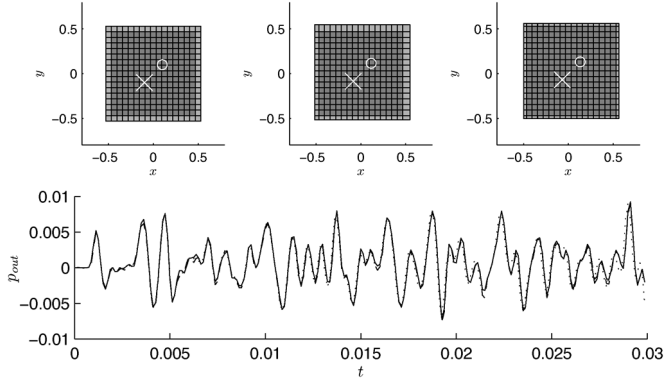


Fig. 8. Time responses for an unrotated but shifted square, in three cases as shown (black, dotted and dashed, respectively). In the first case, at left, the cells are chosen so as to align exactly with the grid; in the second, such that there is a quarter cell offset, and in the third, a half cell offset. Excitation/readout points are indicated on the diagram by \circ and \times respectively, and the excitation is a raised cosine pulse of duration 1 ms, and where the sample rate is 8 kHz. Here, in order to reduce effects of interpolation at input/output locations, 10th order sinc interpolation is used.

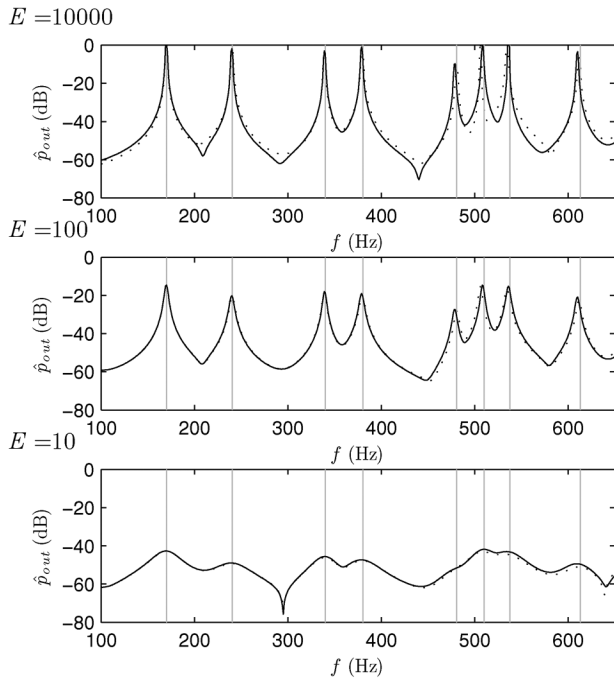


Fig. 9. Frequency responses, under the same geometry and excitation conditions as in Fig. 5, under the boundary condition (11), with $D = F = 0$, and for various values of the loss parameter E , as indicated. Frequency responses are shown under no rotation (dotted line) and under a rotation of 20° (solid line). Fitted boundary cells are employed, and the sample rate is 8 kHz.

boundary. Returning to the case of the rotated square geometry under fixed conditions, at a rotation of 20° , the staircase approximation exhibits a numerical splitting such degenerate mode pairs, as illustrated in Fig. 6. The splitting is not apparent when fitted cells are employed.

As might be expected, the time responses under the fitted boundary approximation show much greater insensitivity to rotation. See Fig. 7.

As another example, consider the case of an unrotated but shifted square, such that cells on opposite sides are possibly not symmetric. Under very accurate interpolation at input and output locations, there is very little distortion of the resulting

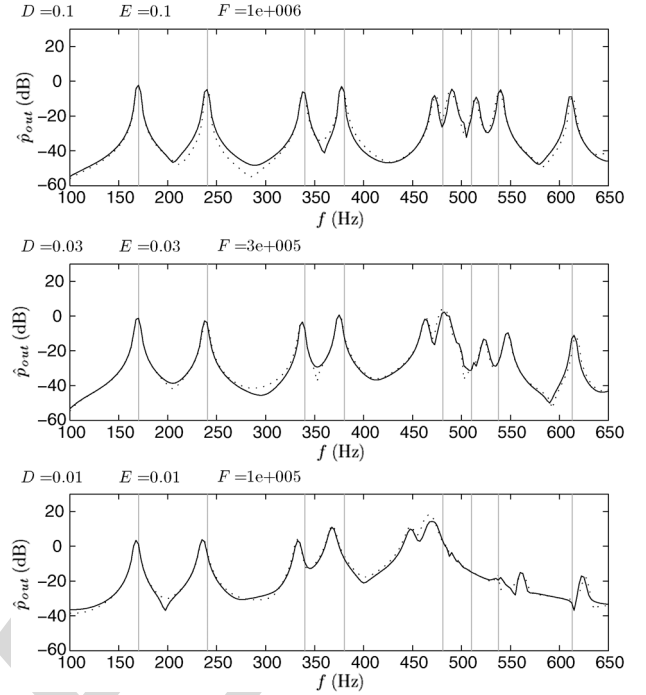


Fig. 10. Frequency responses, under the same geometry and excitation conditions as in Fig. 5, under the boundary condition (11), with values of the parameters D, E, F as indicated. Frequency responses are under no rotation (dotted line) and under a rotation of 20° (solid line). Fitted boundary cells are employed, and the sample rate is 8 kHz.

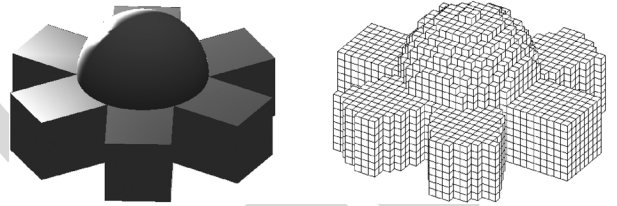


Fig. 11. 3D room geometry (left) and staircase approximation (right). In this case the wall conditions are set to be purely resistive ($A = 0, B = 1, C = 0$ over the dome section and on the floor, and lossless but reactive ($A = 10, B = 0, C = 1$) over all other surfaces.

waveform—as can be seen in Fig. 8, such effects are smaller than the visible effects of numerical dispersion for the scheme itself.

The insensitivity of the fitted scheme to rotation persists under nontrivial boundary conditions, such as, e.g., the series condition (11). See Fig. 9, showing a comparison of frequency responses under different choices of the loss parameter E , with $D = F = 0$, corresponding to a purely resistive termination. A more realistic case is that of a wall admittance possessing a strong resonance (i.e., with the mass and stiffness parameters D and F nonzero), leading to shifts in the locations of the modal frequencies in the region close to resonance. See Fig. 10, where the series condition (11) is again chosen, with a resonance in the admittance of 500 Hz.

C. Complex Room Geometries in 3D

As an example of the use of such schemes over complex geometries in 3D, with variable wall conditions, consider the nontrivial building geometry illustrated in Fig. 11. Boundary conditions are of the parallel type given in (9).

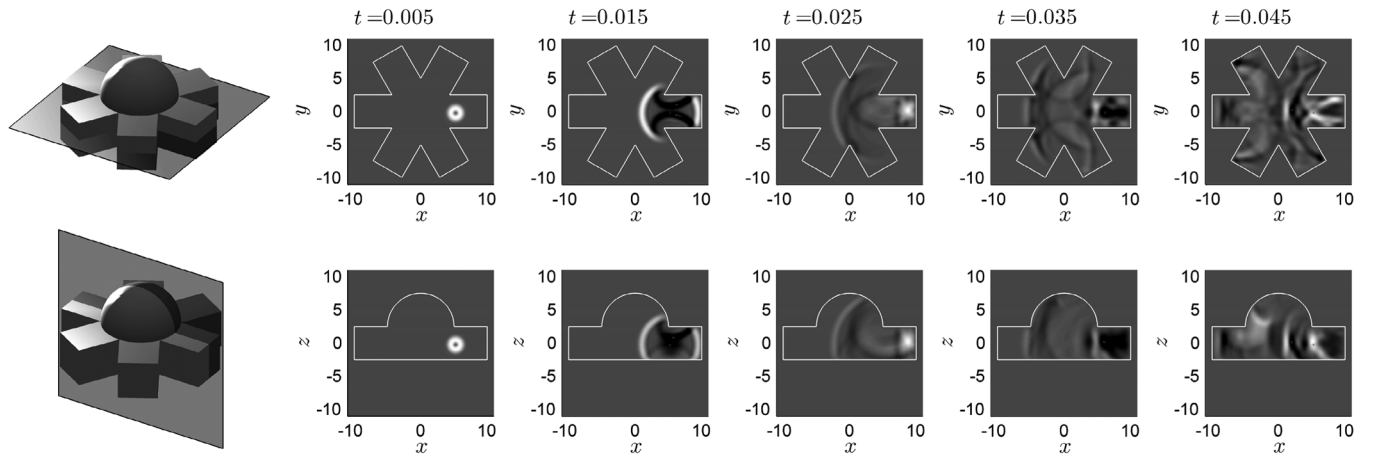


Fig. 12. Snapshots of the time evolution of the acoustic field, at times as indicated, for the room geometry illustrated in Fig. 11. The sample rate is 4 kHz, and the velocity potential is excited with a raised cosine pulse.

TABLE I
NUMERICAL ENERGY CONSERVATION

n	$h_{(i)}^n$	$h_{(b)}^n$	h^n
1	2.14054054054054	0	2.14054054054054
50	2.14022813727786	0.00031240326267	2.14054054054053
100	2.14027272427337	0.00026781626718	2.14054054054054
150	2.14022916409747	0.00031137644307	2.14054054054053
200	2.14016660804255	0.00037393249799	2.14054054054053
250	2.14021042634715	0.00033011419338	2.14054054054053

A series of snapshots of cross sections of the time evolution of the acoustic field (here, Ψ) is shown in Fig. 12.

Under lossless conditions (i.e., if B is set to zero everywhere), the scheme again conserves total energy to machine accuracy, with a portion of the energy stored at the walls if $A, C \neq 0$. See Table I, showing the partition of energy in Joules between that of the acoustic field and that stored at the reactive wall terminations, as a function of time step. It is to be noted that the calculation of numerical energy in the scheme is not necessary in the final simulation algorithm—beyond being a useful theoretical tool in proving numerical stability, however, it is extremely useful as a debugging tool when developing 3D codes. If there is an error in the treatment of a boundary condition (under lossless conditions) then this will be exhibited as an anomalous variation in the numerical energy.

VI. CONCLUDING REMARKS

Methods based on unstructured grids or tilings, such as the finite volume method, have great advantages in real world simulation problems over complex geometries and with nontrivial boundary conditions. In the present case of direct simulation of room acoustics problems, which is a computational task of very large proportions, a reduction of such schemes to regular lattices is at present necessary—but even in this case it becomes possible to approach fine-grained modeling of irregular boundaries within a coherent framework allowing for stability analysis. That being said, for large geometries, and at audio sample rates, a staircase approximation is probably sufficient for room auralization applications, and the boundary stability analysis described here handles this case with ease.

When applied over a regular tiling, as mentioned above, such finite volume methods reduce to nearest neighbor FDTD schemes which have been explored in some depth in the room acoustics literature and the geometrical stability conditions given here in the unstructured case are, in general, only sufficient: for schemes over Cartesian grids, they correspond to bounds obtained using standard stability-checking machinery (such as, e.g., von Neumann analysis for FDTD schemes [24]), but in others (such as the hexagonal tiling discussed in Section IV) are too strict. Such distinctions between sufficient and necessary stability conditions also appear in the consideration of concretely passive stability conditions in waveguide meshes [33], [35]. The question of extending these approaches to attack the problem of accurate boundary termination over complex geometries for more accurate (but less local) FDTD methods (see, e.g., [16], [36], [37]) remains open.

The wall conditions examined here are more general than simple reflective conditions, and incorporate (as in previous work [38]) simple frequency-dependent effects of mass, stiffness and loss. Yet, true wall reflectances are more complex, and will require more detailed modeling. What must remain true, however, is that the boundary condition is passive, and the framework presented here allows for termination by higher order combinations of canonical mass, stiffness and loss elements, perhaps fit to measured data through a network synthesis procedure [27]. Not examined here, however, is the case of diffuse reflection, which has been approached using digital waveguide meshes [39] and FDTD schemes [40].

In parallel realizations, new questions emerge: though it is useful in this regard to retain the regular lattice structure of FDTD, by specializing finite volume approaches to regular polyhedra, the resulting finite difference schemes are thus specialized at the boundary, leading to some departure from an ideal parallel update. Related to this is the need for a general approach to tiling of the boundary which is suitable for audio applications, and which does not add too much additional complexity to an already quite large computational problem. That being said, in terms of a raw operation count and memory requirements, the difference between a crude staircase approximation and a fitted tiling is negligible, and yet leads to great increases in accuracy. Though not ruled out in this article,

use of a fully unstructured grid (perhaps through a Delaunay tessellation of the volume) would have large implications for parallelizability, and most probably negative, especially given the size of the problem in typical room acoustics applications. The stability analysis techniques presented here, however, remain unchanged in the fully unstructured case.

Beyond being used in room acoustics applications, as is the intention here, such methods could also be used as a means of obtaining much better accuracy in scattering problems which appear in audio and acoustics, such as, e.g., the numerical determination of head related transfer functions from measured head geometry [41], using relatively coarse grids at a low audio sample rate.

REFERENCES

- [1] G. Naylor, "Odeon—Another hybrid room acoustical model," *Applied Acoustics*, vol. 38, pp. 131–143, 1993.
- [2] J. Allen and D. Berkley, "Image method for efficiently simulating small-room acoustics," *J. Acoust. Soc. Amer.*, vol. 66, no. 4, pp. 943–950, 1979.
- [3] E. Lehmann and A. Johansson, "Diffuse reverberation model for efficient image-source simulation of room impulse responses," *IEEE Trans. Audio, Speech, Lang. Process.*, vol. 18, no. 6, pp. 1429–1439, Aug. 2010.
- [4] S. Petrausch and R. Rabenstein, "Simulation of room acoustics via block-based physical modeling with the functional transformation method," in *Proc. IEEE Workshop Appl. Signal Process. Audio Acoust.*, New Paltz, NY, USA, 2005, pp. 195–198.
- [5] M. Bansal, W. Ahnert, and S. Feistel, "Large scale FEM analysis of a studio room," in *Proc. Audio Eng. Soc. Conv.*, Paris, France, 2006.
- [6] A. Pietrzyk and M. Kleiner, "The application of the finite-element method to the prediction of soundfields of small rooms at low frequencies," in *Proc. Audio Eng. Soc. Conv.*, Munich, Germany, 1997.
- [7] M. Bai, "Study of acoustic resonance in enclosures using eigenanalysis based on boundary element methods," *J. Acoust. Soc. Amer.*, vol. 91, no. 5, pp. 2529–2538, 1992.
- [8] Y. Horinouchia, T. Osa, K. Murakami, and D. Takahashi, "Application of audience-seats characteristics to the sound field analysis for large enclosures," *Appl. Acoust.*, vol. 68, no. 9, pp. 939–952, 2006.
- [9] J. Hargreaves and T. Cox, "A transient boundary element method model of Schroeder diffuser scattering using well mouth impedance," *J. Acoust. Soc. Amer.*, vol. 124, no. 5, pp. 2942–2951, 2008.
- [10] A. Southern, D. T. Murphy, G. Campos, and P. Dias, "Finite difference room acoustic modelling on a general purpose graphics processing unit," in *Audio Eng. Soc. Conv. 128*.
- [11] R. Mehra, N. Raghuvanshi, L. Savioja, M. Lin, and D. Manocha, "An efficient GPU-based time domain solver for the acoustic wave equation," *Appl. Acoust.*, vol. 73, no. 2, pp. 83–94, 2012.
- [12] C. Webb and S. Bilbao, "Computing room acoustics with CUDA—3D FDTD schemes with boundary losses and viscosity," in *Proc. IEEE Int. Conf. Acoust., Speech, Signal Process. (ICASSP)*, 2011, pp. 317–320.
- [13] J. Sheaffer and B. Fazenda, "FDTD/K-DWM simulation of 3D room acoustics on general purpose graphics hardware using compute unified device architecture (CUDA)," in *Proc. Inst. Acoust.*, 2010, vol. 32, no. 5.
- [14] J. J. López, D. Carnicero, and N. Ferrando, "Parallelization of the finite-difference time-domain method for room acoustics modelling based on CUDA," *Math. Comput. Modell.*, vol. 57, no. 7–8, pp. 1822–1831, 2013.
- [15] D. Botteldooren, "Finite-difference time-domain simulation of low-frequency room acoustic problems," *J. Acoust. Soc. Amer.*, vol. 98, no. 6, pp. 3302–3308, 1995.
- [16] K. Kowalczyk and M. van Walstijn, "Room acoustics simulation using 3-D compact explicit FDTD schemes," *IEEE Trans. Audio, Speech, Lang. Process.*, vol. 19, no. 1, pp. 34–46, Jan. 2011.
- [17] L. Savioja, "Real-time 3D finite-difference time-domain simulation of low- and mid-frequency room acoustics," in *Proc. Int. Conf. Digital Audio Effects*, Graz, Austria, Sep. 2010.
- [18] S. van Duyne and J. O. Smith, III, "Physical modelling with the 2D digital waveguide mesh," in *Proc. Int. Comput. Music Conf.*, Tokyo, Japan, Sep. 1993, pp. 40–47.
- [19] D. Murphy, A. Kelloniemi, J. Mullen, and S. Shelley, "Acoustic modelling using the digital waveguide mesh," *IEEE Signal Process. Mag.*, vol. 24, no. 2, pp. 55–66, Mar. 2007.
- [20] L. Savioja, J. Backman, A. Järvinen, and T. Takala, "Waveguide mesh method for low-frequency simulation of room acoustics," in *Proc. 15th Int. Conf. Acoust.*, Trondheim, Norway, Jun. 1995, pp. 637–640.
- [21] A. Garriga, C. Spa, and J. Escolano, "Impedance boundary conditions for pseudo-spectral time-domain methods in room acoustics," *Appl. Acoust.*, vol. 71, no. 5, pp. 402–410, 2010.
- [22] C. L. Wagner, J. B. Schneider, and R. J. Kruhlak, "Simple conformal methods for finite-difference time-domain modeling of pressure-release surfaces," *J. Acoust. Soc. Amer.*, vol. 104, no. 6, pp. 3219–3226, 1998.
- [23] P. Depalle, J. Lee, G. Scavone, and M. Kim, "Conformal method for the rectangular digital waveguide mesh," in *Proc. IEEE Workshop Appl. Signal Process. Audio Acoust.*, New Paltz, New York, USA, 2011, pp. 293–296.
- [24] J. Strikwerda, *Finite Difference Schemes and Partial Differential Equations*. Pacific Grove, CA, USA: Wadsworth and Brooks/Cole Advanced Books and Software, 1989.
- [25] B. Gustafsson, H.-O. Kreiss, and A. Sundstrom, "Stability theory of difference approximations for mixed initial boundary value problems. II," *Math. Comput.*, vol. 26, no. 119, pp. 649–686, 1972.
- [26] P. Morse and U. Ingard, *Theoretical Acoustics*. Princeton, NJ, USA: Princeton Univ. Press, 1968.
- [27] L. Weinberg, *Network Analysis and Synthesis*. New York, NY, USA: McGraw-Hill, 1962.
- [28] H. Kuttruff, *Room Acoustics*, fourth ed. London, U.K.: Taylor and Francis, 2000.
- [29] A. Mohammadian, V. Shankar, and W. Hall, "Application of time-domain finite-volume method to some radiation problems in two and three dimensions," *IEEE Trans. Magn.*, vol. 27, no. 5, pp. 3841–3844, Sep. 1991.
- [30] R. Leveque, *Finite Volume Methods for Hyperbolic Problems*. Cambridge, U.K.: Cambridge Univ. Press, 2002.
- [31] D. Botteldooren, "Acoustical finite-difference time-domain simulation in a quasi-Cartesian grid," *J. Acoust. Soc. Amer.*, vol. 95, no. 5, pp. 2313–2319, 1994.
- [32] C. Adamsson, J. Nordstrom, K. Forsberg, and P. Eliasson, "Finite volume methods, unstructured meshes and strict stability," *Appl. Numer. Math.*, vol. 45, pp. 453–473, 2003.
- [33] S. Bilbao, *Wave and Scattering Methods for Numerical Simulation*. Chichester, U.K.: Wiley, 2004.
- [34] S. Bilbao, *Numerical Sound Synthesis*. Chichester, U.K.: Wiley, 2009.
- [35] S. Bilbao and J. O. Smith, III, "Finite difference schemes and digital waveguide networks for the wave equation: Stability, passivity and numerical dispersion," *IEEE Trans. Speech Audio Process.*, vol. 11, no. 3, pp. 255–266, May 2003.
- [36] G. Campos and D. Howard, "On the computational efficiency of different waveguide mesh topologies for room acoustic simulation," *IEEE Trans. Speech Audio Process.*, vol. 13, no. 5, pp. 1063–1072, 2005.
- [37] S. Bilbao, "Optimized FDTD schemes for 3-D acoustic wave propagation," *IEEE Trans. Audio, Speech, Lang. Process.*, vol. 20, no. 5, pp. 1658–1663, Jul. 2012.
- [38] K. Kowalczyk and M. van Walstijn, "Modeling frequency-dependent boundaries as digital impedance filters in FDTD and K-DWM room acoustics simulations," *J. Audio Eng. Soc.*, vol. 56, no. 7/8, pp. 569–583, 2008.
- [39] S. Shelley and D. Murphy, "Modeling diffuse boundaries in the 2-D digital waveguide mesh," *IEEE Trans. Audio, Speech, Lang. Process.*, vol. 16, no. 3, pp. 651–655, 2008.
- [40] M. van Walstijn, K. Kowalczyk, and D. Murphy, "A phase grating approach to modeling surface diffusion in FDTD room acoustics simulations," *IEEE Trans. Audio, Speech, Lang. Process.*, vol. 19, no. 3, pp. 528–537, Mar. 2011.
- [41] P. Mokhtari, H. Takemoto, R. Nishimura, and H. Kato, "Computer simulation of HRTFs for personalization of 3D audio," in *Proc. Int. Symp. Universal Commun.*, Osaka, Japan, Dec. 2008.

Stefan Bilbao (B.A. Physics, Harvard, 1992, MSc., PhD Electrical Engineering, Stanford, 1996 and 2001 respectively) is currently a Senior Lecturer in the Acoustics and Audio Group at the University of Edinburgh, and was previously a lecturer at the Sonic Arts Research Centre, at the Queen's University Belfast, and a research associate at the Stanford Space Telecommunications and Radioscience Laboratories. He is currently the leader of the NESS project (Next Generation Sound Synthesis), funded by the European Research Council, and running jointly between the Acoustics and Audio Group and the Edinburgh Parallel Computing Centre at the University of Edinburgh between 2012 and 2017.